Pergamon

Int. J. Heat Mass Transfer. Vol. 38, No. 4, pp. 655–663, 1995

0017-9310/95 $9.50+0.00

0017-9310(94)00190-1

Thermodynamic optimization method of a triple effect absorption system with wasted heat recovery

D. M. MANOLE and J. L. LAGE†

Mechanical Engineering Department, Southern Methodist University, Dallas, TX 75275-0337, U.S.A.

(*Received* 13 *October* 1993 *and in final form* 16 *June* 1994)

Abstract—A detailed performance study is done for a water–lithium bromide triple regenerative effect absorption refrigerating system, with heat recovery. An analysis method is developed and implemented on a computer code to simulate the operation and control of the system under realistic conditions. The thermodynamic performances of the system are described by means of exergetic and energetic based criteria. The numerical results revealed that, by recovering wasted thermal energy into a heating effect, the system global exergetic efficiency is sensibly increased. It is also demonstrated that the amount of heat produced by the system decreases with the temperature of the heating effect while the global exergetic efficiency is increased.

1. INTRODUCTION

The diversity of engineering operations in most industries requires the simultaneous availability of both heating and cooling sources. This is particularly evident in the strategic areas of pharmaceutical and electronics manufacturing. Also in food industries, where several thermal processes coexist, heating and cooling sources are constantly required. In the area of services, for instance hotels, restaurants, etc., next to the cooling requirement for air conditioning, hot water production is generally the most important thermal load.

A thermodynamically efficient choice for obtaining cooling or heating effects is the use of thermally, instead of mechanically, actuated systems. This goal can be achieved with absorption systems, for instance. These systems are also attractive for recovering moderate temperature thermal sources, otherwise wasted.

Recent research interest on absorption systems is partially justified by the need to substitute CFC-based vapor compression systems to reduce the depletion of the ozone layer [1].

Kouremenos *et al.* [2] performed an experimental study of an absorption refrigerating system working with an ammonia–water/water–lithium bromide compound. Best and Hernandez [3] obtained experimentally the operating characteristics of an ammonia–water absorption refrigerating system designed for solar cooling. A solar-assisted heat pump system was studied by Loveday and Craggs [4]. The performance criterion used was the time response of the system to variations of ambient temperature (thermal reservoir). Energetic coefficients of performance and flow ratios for a two-vapor generators water–lithium chloride heat pump system were presented by Won and Lee [5] and compared to a water–lithium bromide solution system.

A proper decision concerning the absorption system configuration is related to the temperature of the available external energetic sources of the cooled or heated medium. Porneala *et al.* [6] presented the ability of recovering low temperature waste heat for different purposes with three thermal absorption or resorption systems.

For obtaining cooling effects at temperatures above water freezing point, water–lithium bromide solution is an advantageous, non-toxic, non-flammable working agent. Porneala [7] studied a two-stage water–lithium bromide absorption refrigeration system whose lower pressure vapor generator recycles the condensing latent heat of the high pressure vapors. A detailed theoretical investigation of a water–lithium bromide two generators absorption refrigerating system was performed by Porneala [8].

Chinnappa [9] demonstrated the possibility of using solar heat source in a water–lithium bromide absorption refrigerating system. In a very interesting work, Eisa [10] studied experimentally the influence of mass flow rate upon the heat load of a water–lithium bromide absorption heat pump.

Research efforts on absorption systems have been geared, generally, towards increasing the overall energetic and exergetic efficiencies by including regenerative heat exchangers. Depending on the number of heat exchangers for heat recycling used, the system is classified as single (one), double (two), triple (three), etc., effect. Evidently, by increasing the number of

†Author to whom correspondence should be addressed.

NOMENCLATURE

Ab	absorber
E	evaporator
G_1	vapor generator 1
G_2	vapor generator 2
H	heating versus cooling effect comparison ratio
i	enthalpy [J kg^{-1}]
K_1	condenser 1
K_2	condenser 2
K_3	condenser 3
$\dot{m}$	mass flow rate [kg s^{-1}]
N	three-way node
p	pressure [Pa]
P_1	pump 1
P_2	pump 2
RHE_1	regenerative heat exchanger 1
RHE_2	regenerative heat exchanger 2
T	temperature [°C]
V	expansion valve
x	concentration.

Greek letters

ε	exergetic
η	efficiency
ϕ	heat flux [J kg^{-1} s^{-1}]
ω	mechanical power [J kg^{-1} s^{-1}].

Subscripts

a	ambient
c	concentrated
d	diluted
e	energetic
i	intermediate.

heat exchangers, the complexity of the system is increased. Although analyses of single and double thermal effect systems have been well documented in the literature [11], little is available on triple effect systems [12], specially when one of the recycling effects is performed within a regenerative vapor generator.

In the present study a triple effect absorption based thermal system that provides, simultaneously, refrigerating and heating effects is analyzed. The heating effect is achieved by recycling the energy necessary for sustaining the refrigerating cycle. This energy is then transferred to a thermal carrier for posterior use. The system is designed also for recovering moderate temperature wasted energy, supposedly available from other thermal processes.

2. TRIPLE EFFECT ABSORPTION SYSTEM

Figure 1 presents the two vapor generators water–lithium bromide absorption system whose performances are studied here. This is a triple effect system since it recycles the input heat by three internal heat transfer processes, respectively, on the regenerative heat exchangers, RHE_1 and RHE_2, and within the secondary vapor generator, G_2. The secondary vapor generator, G_2, is included for recycling and recovering energy, besides providing higher availability heating effect.

The absorber, Ab, delivers the diluted solution at a rate $\dot{m}_2$ and concentration x_d to the primary vapor generator, G_1, that operates at high pressure, p_{K_1}, and temperature, T_{G_1}. Previously, the diluted solution passes through the two regenerative heat exchangers, RHE_1 and RHE_2. Heat load ϕ_{G_1} is applied to G_1 for separating the water vapors at a rate $\dot{m}_3$. The remaining solution goes through the primary regenerative heat exchanger, RHE_1, and delivers a part of its sensible heat to the flow $\dot{m}_2$ supplied to G_1.

Next, the flow $\dot{m}_5$ of water vapors and the flow $\dot{m}_6$ of concentrated solution are separated out of the flow $\dot{m}_1$ within the secondary vapor generator, G_2. The necessary thermal load for the vapor generation process is obtained by condensing the flow $\dot{m}_3$ of high pressure water vapors in the condenser K_1. An additional thermal load, $\phi_{G_2\text{add}}$, supplied to the secondary vapor generator, G_2, is considered for studying the system performances within a larger range of operating parameters. Before going into the absorber Ab, the concentrated solution flow $\dot{m}_6$ transfers heat inside the regenerative heat exchanger RHE_2 to the diluted solution flow $\dot{m}_2$.

The water vapors obtained in the vapor generator

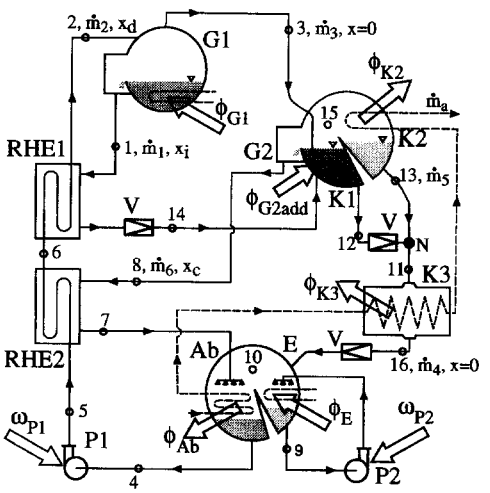

Fig. 1. Two vapor generators water–lithium bromide absorption system (Ab—absorber, E–evaporator, G_1—vapor generator 1, G_2—vapor generator 2, K_1—condenser 1, K_2—condenser 2, K_3—condenser 3, N—three-way node, P_1—pump 1, P_2—pump 2, RHE_1—regenerative heat exchanger 1, RHE_2—regenerative heat exchanger 2, V—expansion valve).

G_2 are condensed in the condenser K_2 and mixed with the water flow $\dot{m}_3$ coming out of condenser K_1. The resulted mixture of vapor and liquid water flow $\dot{m}_4$ goes toward the evaporator E where, at lower pressure, it provides the refrigerating load ϕ_E.

The third condenser, K_3, has the task of condensing the eventual vapors due to an incomplete condensation in K_1 and to supply a saturated water flow at a lower enthalpy to the evaporator E.

An auxiliary flow, $\dot{m}_a$, receives the heat load ϕ_{Ab} from the absorber, and ϕ_{K_3} and ϕ_{K_2} from condensers K_3 and K_2, respectively. In this way, the heat energy $(\phi_{Ab}+\phi_{K_2}+\phi_{K_3})$ can be delivered by the system at a sufficiently high temperature, T_{K_2}, for useful purposes and not just wasted to the environment.

3. ANALYSIS METHOD

Following the method presented by Porneala [13] the number of independent energy or mass balance equations, n_t, is determined by:

$$n_t = \underbrace{n_1+2n_2}_{\text{mass balance}} - \underbrace{k+n_e+s}_{\text{energy balance}} \quad (1)$$

where k is the total number of fluid components in the system, n_1 is the number of nodes of order 1 (nodes where three or more streams, carrying only one constituent, merge), n_2 is the number of nodes of order 2 (nodes where three or more streams, carrying both constituents, merge), n_e is the number of energetic nodes (nodes where three or more streams, with different enthalpies, merge), and s is the total number of surface heat exchangers. For the system shown in Fig. 1, the total number of independent equations obtained from equation (1) is 15, considering: $k = 2$ (lithium bromide and water), $n_1 = 1$ (N), $n_2 = 2$ (Ab, G_1, G_2), $n_e = 5$ (G_1, G_2, K_1, Ab, N), $s = 5$ (RHE_1, RHE_2, P_1, E, K_2, K_3).

Considering isoenthalpic process in the expansion valves, the independent equations (left-most column), and respective node (center column) and unknowns (right-most column) for this system are:

$$\dot{m}_5(i_{15}-i_{13}) = \phi_{K_2} \qquad K_2 \text{ energy equation} \Rightarrow \dot{m}_5$$

$$\left.\begin{aligned} \dot{m}_5+\dot{m}_3 &= \dot{m}_4 \qquad N \text{ mass equation} \\ \dot{m}_5 i_{13}+\dot{m}_3 i_{12} &= \dot{m}_4 i_{11} \qquad N \text{ energy equation} \end{aligned}\right\} \Rightarrow \dot{m}_4, i_{11}$$

$$\dot{m}_4+\dot{m}_6 = \dot{m}_2$$

$$\dot{m}_6 x_c = \dot{m}_2 x_d$$

$$\dot{m}_4 i_{10}+\dot{m}_6 i_7-\dot{m}_2 i_4 = \phi_{Ab}$$

$$\left.\begin{aligned} &Ab \text{ mass equation} \\ &Ab \text{ LiBr mass equation} \\ &Ab \text{ energy equation} \end{aligned}\right\} \Rightarrow \phi_{Ab}, \dot{m}_2, \dot{m}_6$$

$$\dot{m}_1+\dot{m}_3 = \dot{m}_2$$

$$\dot{m}_1 x_i = \dot{m}_2 x_d$$

$$\dot{m}_1 i_1+\dot{m}_3 i_3-\dot{m}_2 i_2 = \phi_{G_1}$$

$$\left.\begin{aligned} &G_1 \text{ mass equation} \\ &G_1 \text{ LiBr mass equation} \\ &G_1 \text{ energy equation} \end{aligned}\right\} \Rightarrow \phi_{G_1}, \dot{m}_1, \dot{m}_3$$

$$\dot{m}_4(i_{11}-i_{16}) = \phi_{K_3} \qquad K_3 \text{ energy equation} \Rightarrow \phi_{K_3}$$

$$\dot{m}_6 i_8+\dot{m}_5 i_{15} = \dot{m}_1 i_{14}+\dot{m}_3(i_3-i_{12})+\phi_{G_2\text{add}}$$

$$G_2-K_1 \text{ energy equation} \Rightarrow \phi_{G_2\text{add}}$$

$$\dot{m}_1(i_1-i_{14}) = \dot{m}_2(i_2-i_6)$$

$$RHE_1 \text{ energy equation} \Rightarrow i_6$$

$$\dot{m}_6(i_8-i_7) = \dot{m}_2(i_6-i_5) \qquad RHE_2 \text{ energy equation} \Rightarrow i_7$$

$$\dot{m}_2(i_5-i_4) = \omega_{P_1} \qquad P_1 \text{ energy equation} \Rightarrow \omega_{P_1}$$

$$\dot{m}_4(i_{10}-i_{16}) = \phi_E \qquad E \text{ energy equation} \Rightarrow \phi_E \quad (2)$$

Pump P_2 has a circulating task, therefore its load is assumed negligible.

Often the calculations for determining an optimal setting of parameters follows the algorithm of selecting the concentrations as variables. In the present study the temperatures are chosen as variables. This choice is based on practical considerations since the computerized control of an absorption system is often based on temperature readings. Furthermore, the concentrations are dependent on the operating temperatures and pressures, with the latter being determined by condensing and evaporating temperatures. The operating temperatures are directly conditioned by the existing interfaces with other energetic systems, thermal loads or environment. By focusing the calculations on different temperature settings the total computational time for simulating the operation of the system is then reduced.

The temperatures T_{G_1}, T_{G_2}, T_{K_1} T_{K_2}, T_{Ab}, T_E, have to be set for establishing the enthalpies that are not considered unknowns but are included in the system of equations (2). In order to limit the ranges of these temperatures, some relations among them are imposed.

For convenience, the absorber operating temperature, T_{Ab}, is considered fixed. Notice that on systems performing the unique useful effect of cooling (no useful heating effect), temperature T_{Ab} is related to the environment temperature, T_a. Temperatures T_{G_1} and T_E are dependent on the external temperature conditions of the hot and cold sources. As it is preferable to focus on the necessary temperature of the vapor generator thermal load, the evaporating temperature, T_E, is also considered constant.

For a chosen value for T_{K_2} we may consider a top limit of T_{G_2}, named $T_{G_2\max}$, as the value for which the concentration x_c of the solution leaving G_2, becomes 0.65. The solution with a concentration beyond this limit is over saturated and susceptible to crystallization at the lower temperatures reached in the second regenerative heat exchanger, RHE_2. A bottom limit for T_{G_2}, named $T_{G_2\min}$, is the value for which the

concentration x_c equals the diluted solution concentration, x_d.

The energetic efficiency of the system can be written as:

$$\eta_e = \frac{\phi_E + \phi_{Ab} + \phi_{K_2} + \phi_{K_3}}{\phi_{G_1} + \phi_{G_2\text{add}} + \bar{\omega}_{P_1,P_2}}. \quad (3)$$

By introducing a parameter representing the energetic ratio between useful heating and cooling effects, H_e, as:

$$H_e = \frac{\phi_{Ab} + \phi_{K_2} + \phi_{K_3}}{\phi_E} \quad (4)$$

the energetic efficiency, equation (3), becomes:

$$\eta_e = (1 + H_e)\frac{\phi_E}{\phi_{G_1} + \phi_{G_2\text{add}} + \bar{\omega}_{P_1,P_2}}. \quad (5)$$

The right-most term of equation (5) is the energetic efficiency of the system (COP) when the recycled heat, $(\phi_{Ab} + \phi_{K_2} + \phi_{K_3})$, is wasted. It follows that the parameter H_e reveals the energetic efficiency increase due to heat regeneration. In terms of COP, the energetic efficiency is: $\eta_e = (1 + H_e)\text{COP}$. Notice that typical COP values for triple stage absorption systems vary in between 1.5 and 1.8 [12]. Since the motto of this study is to present the advantages of recovering heat, attention is focused then on H_e.

The exergetic parameter, H_ε, corresponding to H_e, is obtained by multiplying the right side of equation (4) with the respective exergetic coefficient ratio,

$$H_\varepsilon = \frac{\phi_{Ab} + \phi_{K_2} + \phi_{K_3}}{\phi_E} \frac{\left(1 - \dfrac{T_a}{(T_{K_2} + T_{Ab})/2}\right)}{\left(\dfrac{T_a}{T_E} - 1\right)} \quad (6)$$

where $(T_{K_2} + T_{Ab})/2$ represents the averaged temperature of the auxiliary thermal carrier. Notice that the exergetic losses due to heat transfer processes at finite temperature differences are not considered in equation (6).

The system performance is also appreciated considering the global exergetic efficiency, determined by:

$$\eta_\varepsilon = \frac{\varepsilon_{\phi_E} + \varepsilon_{\phi_{Ab}} + \varepsilon_{\phi_{K_2}} + \varepsilon_{\phi_{K_3}}}{\varepsilon_{\phi_{G_1}} + \varepsilon_{\phi_{G_2\text{add}}} + \omega_{P_1}} \quad (7)$$

where

$$\varepsilon_{\phi_E} = \phi_E\left(\frac{T_a}{T_E} - 1\right) \quad \varepsilon_{\phi_{K_3}} = \phi_{K_3}\left(1 - \frac{T_a}{T_{K_3}}\right)$$

$$\varepsilon_{\phi_{K_2}} = \phi_{K_2}\left(1 - \frac{T_a}{T_{K_2}}\right) \quad \varepsilon_{\phi_{Ab}} = \phi_{Ab}\left(1 - \frac{T_a}{T_{Ab}}\right)$$

$$\varepsilon_{\phi_{G_1}} = \phi_{G_1}\left(1 - \frac{T_a}{T_{G_1}}\right)$$

$$\varepsilon_{\phi_{G_2\text{add}}} = \phi_{G_2\text{add}}\left(1 - \frac{T_a}{T_{G_2}}\right). \quad (8)$$

On the global exergetic efficiency, it has to be considered that, by not using in full the refrigerating or heating effects, the real exergetic efficiency may be strongly compromised. So, equation (7) provides an upper boundary for the exergetic efficiency. A more realistic equation for the exergetic efficiency would have to include the effect of not using the total energetic effect provided by the system, ϕ_{unused}, in which case:

$$\eta_{\varepsilon,\text{real}} = \frac{\varepsilon_{\phi_E} + \varepsilon_{\phi_{Ab}} + \varepsilon_{\phi_{K_2}} + \varepsilon_{\phi_{K_3}} - \varepsilon_{\phi_{\text{unused}}}}{\varepsilon_{\phi_{G_1}} + \varepsilon_{\phi_{G_2\text{add}}} + \omega_{P_1}} \quad (9)$$

where

$$\varepsilon_{\phi_{\text{unused}}} = (\phi_{Ab} + \phi_{K_2} + \phi_{K_3})_{\text{unused}}\left[1 - \frac{T_a}{(T_{K_2} + T_{Ab})/2}\right]$$

or

$$\varepsilon_{\phi_{\text{unused}}} = \phi_{E\text{unused}}\left(\frac{T_a}{T_E} - 1\right) \quad (10)$$

with the first expression related to the unused amount of heating effect and the second term related to the unused amount of cooling effect. Notice that all exergy coefficients are computed using absolute temperatures (K).

A thermodynamic cycle sample of the studied system is presented in Fig. 2. This cycle represents a case whose exact settings and performances are mentioned later on. Notice that, in this particular case, state 14 is identical with state 1, and state 2 is identical to state 6, indicating that the regenerative heat exchanger RHE_1 is not working. Also, states 17 and 18, not depicted in Fig. 1, are saturation states within vapor generators G_2 and G_1 at concentration x_i and x_d, respectively.

A computer code was written for calculating the system's operational behavior under several realistic configurations. Figure 3 shows schematically the algorithm used for performing the calculations. Temperature T_2 of the diluted solution going into the vapor generator G_1 is assumed, initially, equal to $(T_2 = T_{G_1} - 5°\text{C})$, supposing a high degree of sensible heat regeneration from the intermediary and concentrated solutions. If the computation reveals the necessity of an additional thermal load on the second vapor generator, ϕ_{G_2}, temperature T_2 is gradually reduced observing the constraint $T_2 \geqslant T_5$. If $T_2 = T_5$, neither RHE_1 nor RHE_2 are operating. In this case, the separation of a larger vapor flow $\dot{m}_5$, to be condensed in condenser K_2, is prioritized due to its effect on the final temperature increase of the auxiliary thermal carrier, $\dot{m}_a$. The system's ability to supply the requested heating effect depends upon an increase of the thermal load ϕ_{G_1} corresponding to a reduced use of the regenerators.

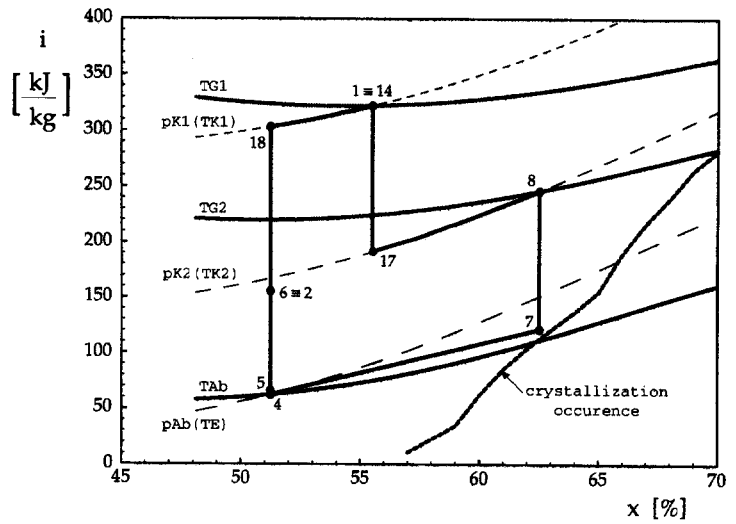

Fig. 2. Thermodynamic cycle in concentration–enthalpy coordinates for $T_{G_1} = 150°C$, $T_{G_2} = 102.53°C$, $T_{K_1} = 105.5°C$, $T_{K_2} = 50°C$, $\eta_\varepsilon = 0.591$.

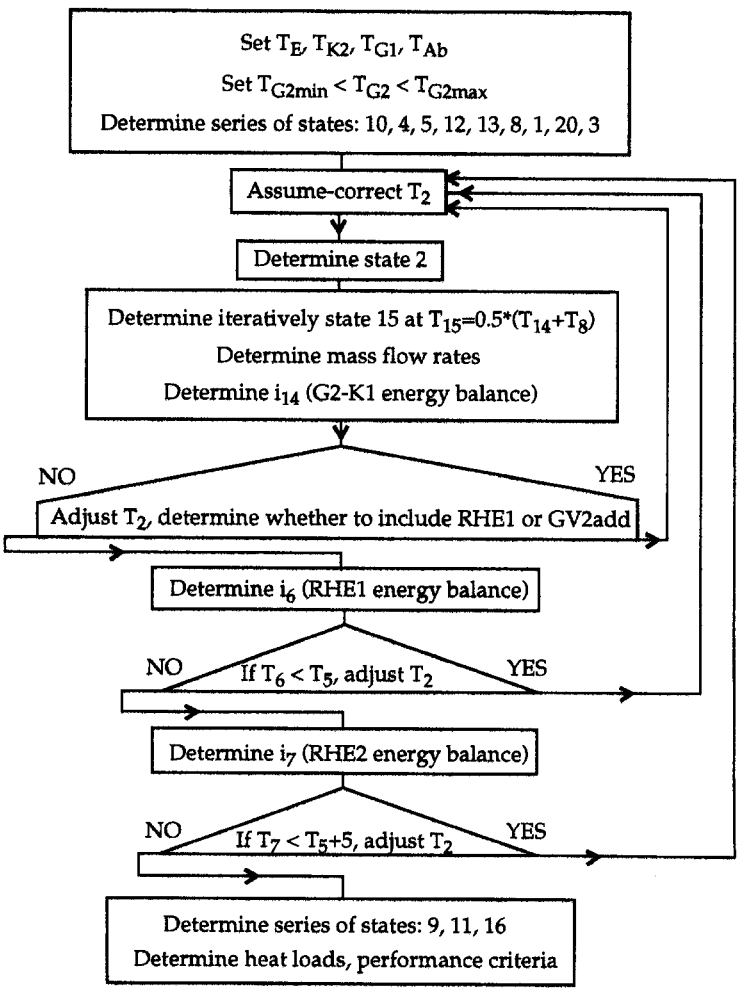

Fig. 3. Scheme of thermodynamic numerical algorithm.

A second test of the T_2 value concerns the occurrence of incomplete condensation within condenser K_1. Eventually, by removing the regenerative heat exchanger RHE_2 it remains the condition $T_6 \geqslant T_5$ that limits the cooling of the intermediary concentration solution.

An internal regenerative heat transfer is preferred for increasing the thermal load of the condenser K_3. Finally, there is a test on whether the resulted internal thermal load of RHE_2, $\dot{m}_5(i_6 - i_5)$, can be supplied by the hotter concentrated solution flow, $\dot{m}_6$.

The code adjusts, with an accuracy of 0.1°C, the temperature of state 2, T_2, and with the same accuracy determines iteratively temperature T_{15}, equal to $(T_8 + T_{14})/2$.

Also a test on crystallization concentration has been made. The curve with the points where the crystallization occurs is represented by the dotted line in Fig. 2.

4. RESULTS AND DISCUSSIONS

Throughout the calculations, the ambient temperature, T_a, is assumed equal to 20°C. The absorbing temperature, T_{Ab}, is considered fixed and equal to 30°C. It is worth noting that these values are not randomly chosen but they follow the general European standard for cooling systems (the American standard is higher, with $T_a = 28$°C and $T_{Ab} = 42$°C.

Temperatures T_{G_1} and T_E are dependent on the external temperature conditions of the hot and cold sources. As we prefer to focus on the necessary temperature of the vapor generator thermal load, the evaporating temperature is also considered constant equal to 7°C, a low temperature that can be efficiently achieved by a water–lithium bromide absorption system.

Figure 4 presents the maximum and minimum values of T_{K_1} vs T_{G_2}, for a set of T_{K_2} temperature values. A minimum T_{K_1} can be considered the value for which the intermediary concentration x_i of the solution delivered to G_2 equals the concentration of the solution leaving the same generator, x_c. When this happens, the second generator does not operate anymore. The results obtained for such a case stand for a system without the subunits K_1–G_2–K_2 among its components.

Temperature $T_{K_1\min}$ can be estimated numerically (°C), by:

$$\begin{aligned} T_{K_1\min} = \operatorname{Max}\{ & -9.35692 + 1.03402 T_{K_2} \\ & + (1.01411 - 0.000401358 T_{K_2}) T_{G_1} \\ & + [-0.694202 - 0.00186886 T_{K_2} \\ & + (-0.00267028 \\ & + 0.0000257561 T_{K_2}) T_{G_1}] T_{G_1}, T_{G_2}\}. \end{aligned} \tag{11}$$

For higher T_{K_2} values (greater than 50°C), the $T_{K_1\min}$ curves present a bending corresponding to T_{K_1} equal to T_{G_2}. The rightmost points of $T_{K_1\min}$ curves, corresponding to $T_{G_2\max}$, are marked with a plus (+) symbol.

The maximum allowable value of condensation temperature in T_{K_1} is limited by the maximum pressure at which the vapor generator G_1 may operate at temperature T_{G_1}, respectively at the limit when state 1 is identical to state 18 (Fig. 2) and $x_i = x_d$. The maximum value of T_{K_1} plotted in Fig. 4, which is a function of T_{G_1} and T_E, can be approximated numerically by:

$$T_{K_1\max} = (-26.1242 + 0.917631 T_E) + 0.895519 T_{G_1}. \tag{12}$$

Equations (11) and (12) provide a very accurate approximation for T_{K_1} with T_{G_1} and T_{K_2} between 120 and 160°C, and 30 and 70°C, respectively.

Varying T_{K_2}, the interval of compatible temperatures T_{K_1}, presents a maximum width. The width of the T_{K_1} values range shows the system liability on operating when the internal parameters (mass flow rates, heat recovering degree within RHE_1 and RHE_2) may vary. These variations occur due to the heat exchanger efficiency depreciation, maintenance or control operations.

However, the numerical computation has been done only for settings that accommodate a minimum concentration increase of 3% within the vapor generators. Otherwise, the cost of additional devices and the increasing complexity of system operation are considered practically unjustified. Figure 5 shows the range of values for temperature T_{K_1} in this case. The maximum T_{K_1} is lowered with the direct effect of reducing the system's ability of operating at the higher values of T_{K_2}. Lower value of $T_{K_1\max}$ induces higher values for $T_{G_2\max}$. Consequently, T_{K_1} can reach lower minimum values as shown in Fig. 5.

Besides equations (11) and (12), equations for calculating the thermodynamic properties [14, 15] are implemented.

Figures 6–8 show the performance parameters of the system vs T_{K_1}, for increasing values of hot source

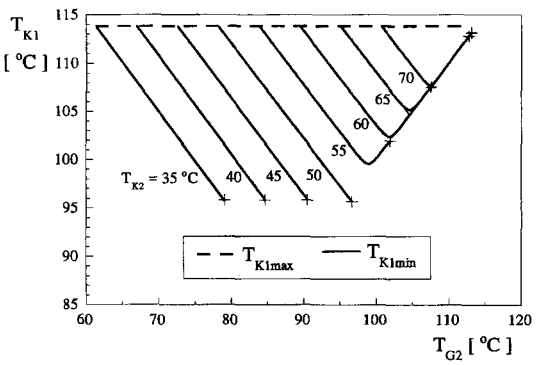

Fig. 4. Temperature T_{K_1} range for $T_{G_1} = 150$°C.

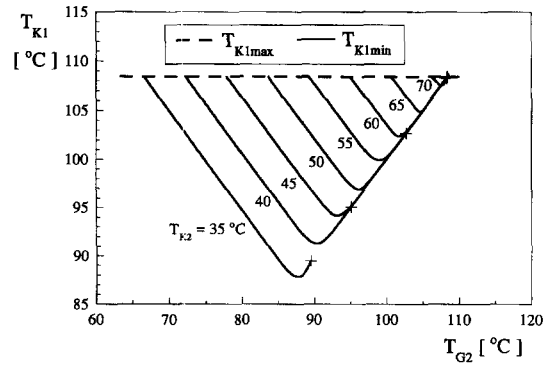

Fig. 5. Temperature T_{K_1} range for $T_{G_1} = 150°C$, subject to the restrictions $(x_c - x_i) \leqslant 0.3$ and $(x_i - x_d) \leqslant 0.3$.

temperature, T_{G_1}. On the abscissa, T_{K_1} varies from $T_{K_1\min}$ to $T_{K_1\max}$ as determined with equations (3) and (4) and shown in Fig. 4. Results are plotted for T_{G_2} temperature varying in between,

$$T_{G_2\min} + (T_{G_2\max} - T_{G_2\min})/3 \leqslant T_{G_2} \leqslant T_{G_2\max}. \quad (13)$$

The arrows point towards crescent values of T_{G_2}. Extreme T_{G_2} values, as well as the temperature increment between successive lines, are listed in the caption of each figure.

On the top graph of Figs. 6–8, a comparison between the moderate and high temperature thermal loads of the vapor generators, respectively $\phi_{G_2\text{add}}$ and ϕ_{G_1}, is presented. The higher the value of T_{K_1}, the larger is the ratio $\phi_{G_2\text{add}}/\phi_{G_1}$ for a particular T_{G_2}. This is advantageous because $\phi_{G_2\text{add}}$ is assumed to be a moderate temperature heat source. By increasing T_{G_2} the additional heat load $\phi_{G_2\text{add}}$ might become greater than zero, in which case the regenerative heat exchanger RHE_1 is not utilized. This indicates that, from this point on, the current system operates as a double effect system. Notice also that when increasing

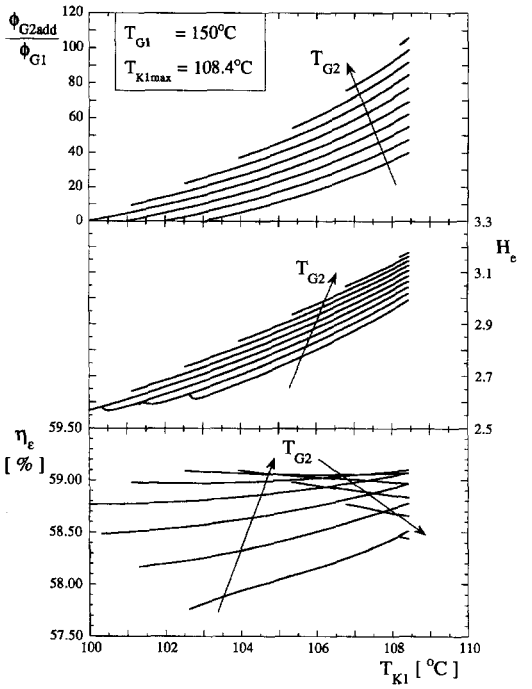

Fig. 7. Combined plots of system performances vs T_{K_1} for T_{G_2} from 95.93°C to 108.19°C in equal intervals of 1.36°C.

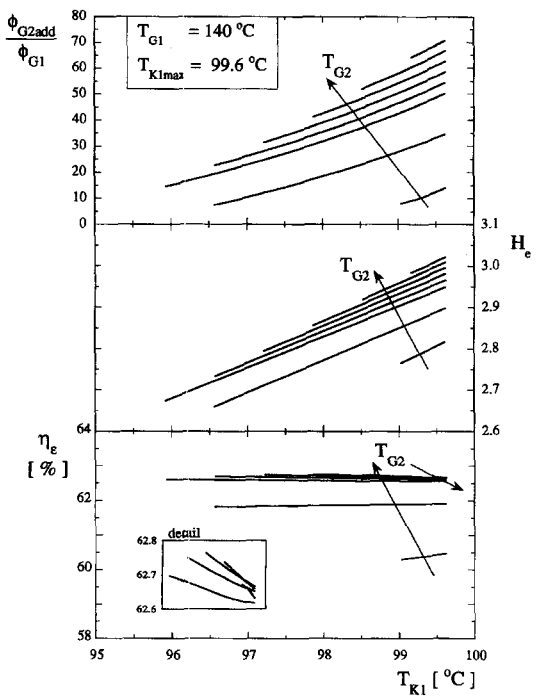

Fig. 6. Combined plots of system performances vs T_{K_1} for T_{G_2} from 90.55°C to 99.17°C in equal intervals of 1.23°C.

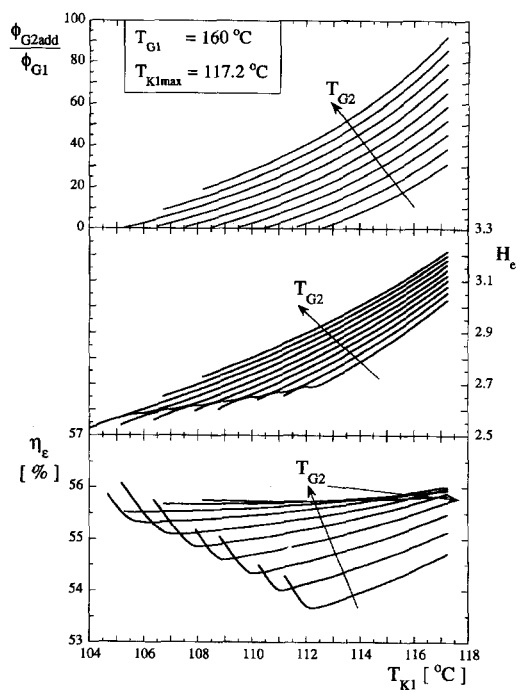

Fig. 8. Combined plots of system performances vs T_{K_1} for T_{G_2} from 95.93°C to 108.90°C in equal intervals of 1.44°C.

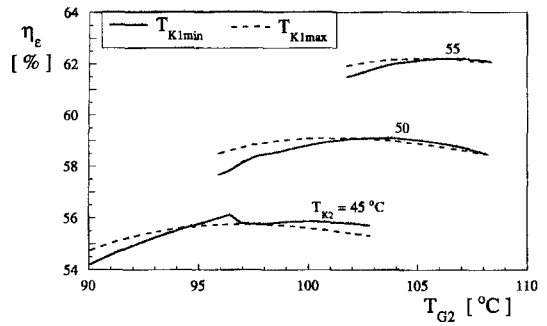

Fig. 9. Exergetic efficiencies vs T_{G_2} at $T_{K_1} = T_{K_1\min}$, and $T_{K_1} = T_{K_1\max}$, for $T_{G_1} = 150°C$.

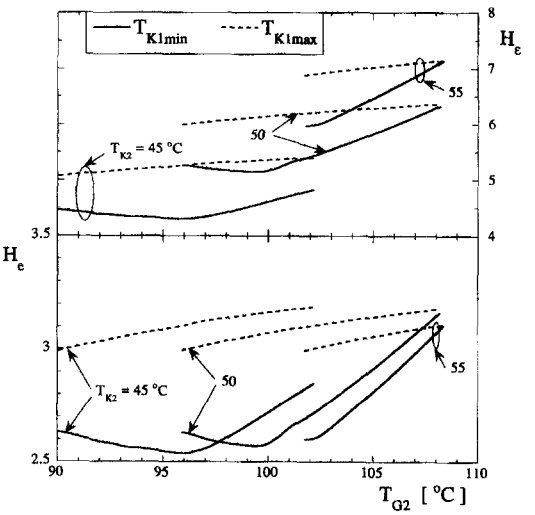

Fig. 10. Energetic (bottom) and exergetic (top), H, ratios vs T_{G_2} at $T_{K_1} = T_{K_1\min}$, and $T_{K_1} = T_{K_1\max}$, for $T_{G_1} = 150°C$.

T_{G_1} the use of the regenerative heat exchanger, RHE_1, becomes necessary for a broader range of T_{K_1}.

The ratio between heating and cooling effects, H_e, is plotted in the middle graph of Figs. 6–8. Increasing T_{G_2}, the refrigerating effect ϕ_E is increased compared to the heating effect $(\phi_{Ab} + \phi_{K_2} + \phi_{K_3})$. The H_e value varies between 2.5 and 3.2, being consistently greater than 1.

On each figure, the bottom graph presents the exergetic efficiency calculated with equation (8). Values of T_{G_2} nearer the minimum compatible value, $T_{G_2\min}$, produce very low exergetic efficiencies and therefore are not considered within the plot. The existence of an optimum T_{G_2}, for maximum exergetic efficiency, is revealed.

It is worth noting that when T_{K_1} is near its minimum value, the additional heat load is no longer necessary, Fig. 8 (top). In this range of T_{K_1} values the RHE_1 is working, as reflected by the negative slope of the exergetic efficiency curves of Fig. 8 (bottom).

In Fig. 9 the exergetic efficiency, η_ε, is presented vs T_{G_2} varying within the limits mentioned in equation (13). For T_{K_1} equal to both, $T_{K_1\min}$ or $T_{K_1\max}$, maximum exergetic efficiency values are found. Increasing T_{K_2}, the exergetic efficiency increases linearly while the operational range of T_{G_2} is reduced.

As presented in Fig. 10, bottom graph, the value of H_e generally decreases for increasing T_{K_2}. This is reversed when T_{G_2}, T_{K_2}, and T_{K_1} are all small, a disadvantageous situation as indicated previously. However, the second term of equation (6) increases with T_{K_2} in a larger amount and therefore parameter H_ε presents a sensible increase with T_{K_2}. That means that, although by increasing T_{K_2} the energetic heating effect is reduced, its exergetic assistance, H_ε, causes an enhancement of the global exergetic efficiency, η_ε, as seen in Fig. 9.

4. CONCLUSIONS

In the present study, optimum sets of operating parameters for a triple effect absorption based thermal system that provides, simultaneously, refrigerating and heating effects are determined. The heating effect is achieved by recycling the energy necessary for sustaining the refrigerating cycle. This energy is then transferred to a thermal carrier for posterior use.

The system is designed for allowing recovery of moderate temperature wasted energy, $\phi_{G_2\text{add}}$, from other processes. It is interesting to note that when this extra energy source is not available the system switches to a triple effect thermal system with RHE_1 coming into play.

Numerical results are related directly to the temperature of the working fluid tackling the problem of setting the operating parameters more realistically. In practice temperature and pressure are more often used as control parameters.

The temperature of the primary vapor generator, T_{G_1}, influences the condensing temperature range, T_{K_1}, one of the practical constraints of the system. The T_{K_1} range reflects the flexibility of the system to operate under different settings. Variations of T_{K_1} occur, not only accidentally, but also when the power of the system is dynamically controlled and therefore the vapor flow $\dot{m}_3$ varies.

Also, the secondary vapor generator temperature, T_{G_2}, has a strong effect upon the T_{K_1} range (see Figs. 3 and 4). The performance analysis suggests the existence of an optimum T_{G_2}, leading to maximum energetic efficiency, for each T_{K_1}.

A proper setting of temperature T_{K_2} can lead to a regime whose exergetic efficiency is almost constant when varying T_{K_1}. Furthermore, the results indicate that by increasing T_{K2} the energetic heating effect, H_e, is reduced while the exergetic assistance, H_ε, is increased, causing an enhancement of the global exergetic efficiency of the system, η_ε. This means that, considering the same cooling effect, less heating energy is obtained, but at a higher quality.

Notice that, in the present configuration, the absorber temperature is constrained by the minimum temperature of the heat recovery stream. For situations where the heat recovery stream comes from

another thermal system at higher temperature (higher than the ambient temperature) it might be more advantageous to recover heat only from the condensers, K_2 and K_3.

Acknowledgements—The authors benefited from helpful discussions with Professor S. Porneala of University of Galati (Romania). Dr Manole acknowledges with gratitude the PhD Scholarship provided by the Mechanical Engineering Department of Southern Methodist University. Professor Lage's work is supported by Southern Methodist University through the J. L. Embrey Professorship in Mechanical Engineering.

REFERENCES

1. S. Somasundaram, M. K. Drost, D. R. Brown and Z. I. Antoniak, Integrating thermal energy storage in power plants, *Mech. Engng* **115**, 84–90 (1993).
2. D. A. Kouremenos, E. Rogdakis and K. A. Antonopoulos, A high-efficiency, compound NH_3/H_2O–H_2O/LiBr absorption–refrigeration system, *Energy* **14**, 893–905 (1989).
3. R. Best and J. Hernandez, Experimental studies on the operating characteristics of an ammonia–water absorption system for solar cooling, *Trans. I. Chem. E.* **69A**, 153–160 (1991).
4. D. L. Loveday and C. Craggs, Stochastic modeling of temperatures affecting the *in situ* performances of a solar-assisted heat pump: the univariante approach, *Solar Energy* **49**, 279–287 (1992).
5. S. H. Won and W. Y. Lee, Thermodynamic design data for double-effect absorption heat pump systems using water–lithium chloride-cooling, *Heat Recovery Syst. CHP* **11**, 41–48 (1991).
6. S. Porneala, D. M. Manole and J. L. Lage, Resorption and absorption systems for recovery of low temperature wasted energy, *Proceedings, ASME Winter Annual Meeting*, New Orleans (1993).
7. S. Porneala, Comments on lithium bromide–water absorption refrigerating systems, *Revista de Chimie* **31**(6), 591–594 (1980) (in Romanian).
8. S. Porneala, Installation frigorifique à absorption eau–bromure de lithium à deux bouilleurs, *Rèvue Gènerale du Froid* **6**, 383–388 (1985).
9. J. C. V. Chinnappa and N. E. Wijeysundera, Simulation of solar-powered integrated hybrid cooling system, *J. Solar Energy Engng.* **114**, 125–127 (1991).
10. M. A. R. Eisa, Heat and mass transfer studies on water–lithium bromide absorption heat pump systems, *Int. J. Heat Mass Transfer* **34**, 891–894 (1991).
11. F. Ziegler and P. Riesch, Absorption cycles: a review with regard to energetic efficiency, *Heat Recovery Syst. CHP* **13**, 147–159 (1993).
12. R. C. De Vault, Advanced absorption technology development in the United States. In *Proceedings of the Third International Energy Agency Heat Pump Conference Heat Pumps: Solving Energy and Environmental Challenges*, pp. 65–80. Pergamon Press, Oxford (1990).
13. S. Porneala, Operating parameters computation of thermo energetic systems, *Revista de Chimie* **27**(3), 223–230 (1976) (in Romanian).
14. *Refrigerent Tables and Charts, ASHRAE Fundamentals Handbook*, Chaps. 16–17 (1981).
15. A. M. Lowell, Thermodynamics properties of aqueous solutions of lithium bromide, *ASHRAE Trans.* **85**, Part 1, 413–434 (1979).